RAMReS Sciences des Structures et de la Matière Vol. 9, N°2 (2025) 289 - 307
http://publication.lecames.org/index.php/mat ISSN: 2630-1180

Potassium-doped kaolinitic clay from Agboville (Côte d'Ivoire): structural characterization, adsorption behavior, and thermodynamic insights

Medy Camille Nongbé[1,2,*], Ehu Camille Aka[3], Marie Jeanne Ohou[1], Mawa Koné[2,4], Tchirioua Ekou[5], Lynda Ekou[5], Abollé Abollé[5]

[1]*Laboratory of Environmental Sciences and Technologies (LSTE) / Jean Lorougnon Guédé University, Côte d'Ivoire*
[2]*National Laboratory for Quality Testing, Metrology and Analysis (LANEMA), (Côte d'Ivoire)*
[3]*Oceanographic Research Center (CRO), Côte d'Ivoire*
[4]*Laboratory of Matter Constitution and Reaction (LCRM) / Félix Houphouët-Boigny University, Côte d'Ivoire*
[5]*Laboratory of Thermodynamics and Physico-Chemistry of the Environment (LTPCM) / Nangui Abrogoua University, Côte d'Ivoire*

Received: 06 September 2025 / Received in revised form: 17 November 2025 / Accepted: 12 December 2025

***Abstract*:**

This study investigates the adsorption of potassium ions onto thermally activated kaolinitic clay from Agboville (Côte d'Ivoire), with emphasis on the influence of particle size and precursor type (K_2CO_3 vs. CH_3CO_2K). The 100–250 μm fraction exhibited the highest performance, with maximum adsorption capacities of 149.84 mg g^{-1} (K_2CO_3) and 198.91 mg g^{-1} (CH_3CO_2K), the latter providing the most efficient uptake. Potassium acetate produced the most homogeneous and effective incorporation of K^+, and was therefore selected as the reference system for further interpretation. The Temkin isotherm model gave the best fit (R^2 = 0.9894), while adsorption kinetics followed the pseudo-second-order model (R^2 = 0.998), indicating a chemisorption-controlled mechanism. Thermodynamic parameters (ΔG° = -6.16 to -8.55 kJ mol^{-1}; (ΔH° = +17.8 kJ mol^{-1}; (ΔS° = +80.3 J mol^{-1} K^{-1}) confirmed a spontaneous and endothermic process. Characterization analyses revealed surface and bonding modifications induced by potassium doping: attenuation of ν(OH) bands (3695–3620 cm^{-1}) and a shift of the ν(Si-O) vibration to ~ 1010 cm^{-1} (FT-IR), an increase in pH_{PZC} from 4.6 to 6.2, homogeneous K^+ distribution (1.0–3.0 at. %, EDS), and thermal stability above 700 °C (TGA/DTG). Overall, potassium-doped Agboville clay, particularly when prepared with CH_3CO_2K, appears as a low-cost, thermally robust and highly basic local adsorbent suitable for aqueous pollutant removal and catalytic support applications.

Keywords **:** Kaolinitic clay ; Potassium doping ; Adsorption kinetics ; Physicochemical characterization.

* Corresponding author:
Email address: *medycamille@gmail.com (M.C. Nongbé)*
https://doi.org/10.70974/mat09225289

1. Introduction

Adsorption using clay-based materials represents an effective, low-cost, and eco-friendly strategy for removing ions or preparing catalytic supports, owing to their abundance, tunable surface chemistry, and ability to undergo physical or chemical activation [1, 2]. In kaolinitic clays, thermal activation plays a central role: between 400 and 600 °C, partial dehydroxylation and removal of organic matter occur, generating a reactive metakaolinite phase characterized by enhanced surface reactivity and modified acid-base properties [3, 4].

Two key parameters govern potassium dispersion and adsorption efficiency on activated clays: particle size and precursor nature [5]. Particle size determines the extent of external surface accessibility and the degree of particle agglomeration. Very fine particles (< 100 µm) tend to agglomerate and reduce the effective contact surface, whereas coarse particles (> 500 µm) offer limited external surface. Intermediate granulometric fractions (100–250 µm) generally provide the most favorable compromise between accessibility and diffusion pathways [6, 7]. The nature of the doping precursor also plays a critical role: potassium acetate, due to its higher solubility and clean thermal decomposition near 350 °C, typically favors more homogeneous K^+ incorporation, whereas potassium carbonate may lead to less uniform distribution because of its stronger alkalinity and slower decomposition.

Modeling adsorption data using Langmuir, Freundlich, and Temkin equations helps elucidate the interactions between adsorbate and adsorbent. More complex three-parameter models (e.g., Toth, Redlich-Peterson, Radke-Prausnitz) may provide better descriptions for heterogeneous surfaces [6]. Likewise, kinetic models, particularly the pseudo-second-order model, are valuable for identifying chemisorption-driven mechanisms [8, 9]. Thermodynamic parameters such as ΔG°, ΔH°, and ΔS° offer further insight into the feasibility, energetic nature, and interfacial changes associated with adsorption processes [10–12].

In this work, we investigate the adsorption behavior of potassium ions on thermally activated kaolinitic clay from Agboville (Côte d'Ivoire), focusing on the influence of particle size and precursor type (K_2CO_3 versus CH_3CO_2K). A comprehensive experimental approach, combining FT-IR spectroscopy, Thermogravimetric Analysis, EDS elemental mapping, and adsorption modeling (kinetic, isothermal, and thermodynamic), was employed. The aim is to determine how granulometry and precursor chemistry govern K^+ retention, dispersion, and stability, thereby demonstrating the potential of this local kaolinite as a low-cost, thermally robust adsorbent and catalytic support.

2. Materials and methods

2.1. Materials

The kaolinitic clay used in this study was collected from the Agboville region (Côte d'Ivoire; 5°55' N, 4°13' W). Potassium carbonate (K_2CO_3, Merck) and potassium acetate (CH_3CO_2K, Sigma-Aldrich) served as doping precursors. Hydrochloric acid (37 %, Prolabo) was used to adjust pH. Grinding and sieving were performed with an IKA M20 mill and a Retsch AS 200 sieve (100–500 µm). Calcination was carried out in a Nabertherm muffle furnace at 400 °C for 3 h, a temperature chosen to obtain partial dehydroxylation while preserving structural integrity. The doped samples were dried at 105 °C (Memmert oven). Potassium quantification was achieved using a Thermo Scientific ICE 3300 atomic absorption spectrometer (AAS) operated with an air-acetylene flame at the LAPISEN facility (INP-HB, Yamoussoukro).

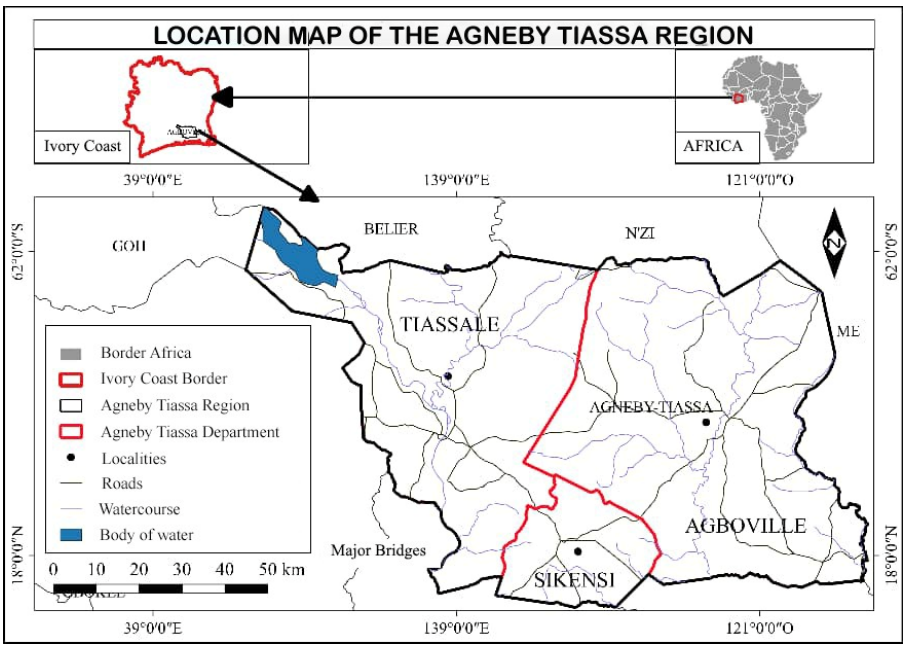

Fig. 1. Map of clay sampling site.

2.2. Methods

2.2.1. Preparation of the calcined clay

The raw Agboville clay (> 2 µm particles) was calcined at 400 °C for 3 h in a muffle furnace, then cooled in a desiccator. The material was ground and sieved into five particle-size fractions: X > 500 µm, 400 < X < 500 µm, 250 < X < 400 µm, 100 < X < 250 µm, and X < 100 µm.

2.2.2. Impregnation procedure

For each experiment, 1.2 g of calcined clay were contacted with 25 mL of an aqueous potassium salt solution (CH_3CO_2K or K_2CO_3) prepared at a 35% K mass ratio relative to the clay. The solution pH was adjusted to different values using dilute HCl or KOH solutions to evaluate the effect of pH on the impregnation process. The mixture was magnetically stirred for 12 h at room temperature, then filtered, and the resulting solid was dried at 105 °C for 2 h before being stored in a desiccator for subsequent analyses.

2.2.3. Determination of potassium content

Each doped sample (0.3 g) was digested in 4 mL aqua regia (HCl : HNO_3 = 3 : 1 v/v) at 100 °C for 2 h. After cooling, a small amount of boric acid was added to neutralize residual acid. The solution was filtered, diluted to 50 mL with deionized water, and analyzed by AAS. The potassium content (mg kg^{-1} dry solid) was calculated from:

$$C_{\text{solid}} = \frac{V_{\text{final}} \times C_{\text{solution}}}{m_{\text{sample}}} \quad (1)$$

where C_{solution} is the measured concentration (mg L^{-1}), V_{final} is the final digest volume (L), and m_{sample} is the dry mass (kg).

2.2.4. Adsorption experiments

Batch adsorption tests were performed at 25 °C with 100 mL solutions of known initial K^+ concentrations. The adsorbent dose was 1 g L^{-1}. After equilibration, suspensions were filtered and analyzed by AAS. The equilibrium capacity (q_e, mg g^{-1}) was determined from:

$$q_e = \frac{V(C_i - C_e)}{m} \quad (2)$$

where C_i and C_e are the initial and equilibrium concentrations (mg L^{-1}), V the solution volume (L), and m the adsorbent mass (g).

2.2.5. Adsorption isotherm modeling

– Langmuir model

This model assumes monolayer adsorption on a homogeneous surface with a defined maximum capacity:

$$q_e = \frac{q_{\max} K_L C_e}{1 + K_L C_e} \quad (3)$$

where q_e is the amount adsorbed at equilibrium (mg g^{-1}), C_e is the equilibrium concentration in solution (mg L^{-1}), q_{max} is the maximum adsorption capacity (mg g^{-1}), and K_L is the Langmuir constant (L mg^{-1}).

– **Freundlich model**

$$q_e = K_F C_e^{1/n} \quad (4)$$

where K_F is the adsorption capacity constant (L mg^{-1}), and n is the adsorption intensity (adsorption is favorable when $1 < n < 10$).

– **Temkin model**

This model accounts for the linear decrease in adsorption heat as surface coverage increases:

$$q_e = B \ln(AC_e) \quad \text{with} \quad B = \frac{RT}{b} \quad (5)$$

where A is the Temkin constant related to adsorption capacity, b is the constant related to adsorption heat, R is the universal gas constant (8.314 J mol^{-1} K^{-1}), and T is the absolute temperature (K).

2.2.6. Kinetic modeling

– **Pseudo-first-order model**

This model assumes that the adsorption rate is proportional to the residual concentration of available sites. Using the experimental data and the linearized kinetic equation:

$$\ln(q_e - q_t) = \ln(q_e) - k_1 t \quad (6)$$

– **Pseudo-second-order model**

The pseudo-second-order model is based on the assumption that adsorption is governed by chemical interactions (covalent or surface bonding). The linear form of the equation is:

$$\frac{t}{q_t} = \frac{1}{k_2 q_e^2} + \frac{t}{q_e} \quad (7)$$

2.2.7. Materials characterization

– **Point of zero charge (pH_{PZC})**

The pH_{PZC} was determined by the pH-drift method (0.01 M NaCl background, initial pH_0 = 2–11 adjusted with 0.1 M HCl/NaOH, clay dose 1.0 g L^{-1}, 24 h equilibration at 25 °C). pH_{PZC} is taken at the intersection where $\Delta pH = pH_f - pH_0 = 0$.

– **FT-IR spectroscopy**

FT-IR spectra were recorded using KBr pellets in the range of 4000–400 cm^{-1}, with a resolution of 4 cm^{-1} and 32 scans. The analyzed samples included: the raw clay, the calcined clay, the K/Clay-CH_3CO_2K.

– **TGA and EDS analyses**

Thermogravimetric analysis (TGA) was performed under a nitrogen atmosphere (N_2) from 25 to 900 °C at a heating rate of 10 °C min^{-1}. Polished powder samples were examined using EDS point analysis and area mapping. For each sample, at least five regions (~100 µm × 100 µm) were mapped to quantify the spatial distribution of potassium (K).

3. Results and discussion

3.1. Influence of clay granulometry on K/Clay adsorption capacity

The granulometry of the clay support is a determining parameter in the process of impregnation and fixation of potassium ions (Table 1). It directly affects the specific surface area, porosity, and internal diffusion of ions within the matrix [13]. Fine particles (X < 100 µm) offer a larger specific surface area, but are more prone to agglomeration and reduction of interparticle porosity, limiting the homogeneous penetration of the precursor solution [14]. Conversely, coarser particles (> 500 µm) have a small specific surface area and therefore fewer active sites available for K^+ fixation. The results obtained show that the particle size range 100 < X < 250 µm is optimal for the potassium adsorption capacity on clay modified by calcination, with maximum values of 149.84 mg g^{-1} for K_2CO_3 and 198.91 mg g^{-1} for CH_3CO_2K. This particle size range provides an ideal compromise between sufficient external surface area and well-connected internal porosity, allowing efficient precursor diffusion and maximum interaction with exchange sites [15].

Table 1
Influence of granulometry on the maximum adsorption capacity of K/Clay.

Granulometry (μm)	K_2CO_3 (mg g^{-1})	CH_3CO_2K (mg g^{-1})	Observation
$X > 500$	122.01	150.18	Low active surface area, limited diffusion
$400 < X < 500$	107.57	186.47	Moderate diffusion, partial internal porosity
$250 < X < 400$	117.59	186.32	Good compromise but lower external surface area
$100 < X < 250$	149.84	198.91	Optimum – balance between surface area and porosity
$X < 100$	125.99	189.32	High surface area but agglomeration and heterogeneity

These results are in agreement with the work of Shaban [16] and Lokman [17], who report that intermediate granulometries optimize metal dispersion by impregnation and minimize pore blocking or surface precipitation phenomena. Thus, controlling the particle size of the support is an essential lever for optimizing final catalytic performance.

3.2. Surface modification of clay by calcination

Calcination is a key step in the preparation of clay supports intended to receive a metallic or alkaline deposit by impregnation. This thermal treatment, generally performed between 300 and 700 °C, induces partial or total dehydroxylation of aluminosilicate layers, removal of organic matter, and decomposition of thermally unstable species [18]. These transformations modify the surface chemistry of kaolinite and generate a more reactive metakaolinite phase, characterized by a higher density of exposed structural sites capable of interacting with cationic species [14].

In our study, calcination of Agboville clay at 400 °C for 3 h produced a material with modified surface properties that favored potassium uptake from K_2CO_3 and CH_3CO_2K solutions. Thermal activation reduces interlayer water content, increases structural disorder at the local scale, and exposes hydroxyl groups and Lewis acid sites created during dehydroxylation. These changes enhance the interaction between the clay surface and added potassium salts, facilitating their retention and stabilization during impregnation.

According to the literature, calcination may also induce partial migration or reorganization of exchangeable cations (Na^+, Ca^{2+}, Mg^{2+}), producing vacant sites with higher affinity for incoming metal ions [17]. Combined with the removal of moisture and reduction of surface-bound impurities, this favors a more uniform distribution of alkaline ions and limits the formation of localized aggregates during drying or subsequent heating steps [16]. Our results show that potassium dispersion is markedly improved when calcination is performed prior to impregnation, in agreement with Alkhabbas, who demonstrated that thermal pretreatment strengthens the ability of clay matrices to stabilize metal deposits [13].

Additionally, the nature of the precursor significantly influences the final amount of potassium fixed on the clay. Potassium acetate, due to its higher solubility and cleaner thermal decomposition, diffuses more efficiently within the activated structure than potassium carbonate, which explains the higher adsorption capacities observed in our

experiments.

Thus, calcination appears as an essential step to prepare the clay surface to receive a potassium deposit by impregnation, optimizing both the pore structure, surface chemistry, and reactivity towards the precursor.

3.3. Influence of pH on K dispersion on calcined clay

pH plays a determining role in the process of dispersion and retention of potassium ions on calcined clay. Indeed, the surface of clay minerals is characterized by edge hydroxyl groups (–Si–OH and –Al–OH) whose net charge varies according to pH (Table 2). At acidic pH, protonation of these groups limits cationic adsorption by competition with H^+ ions, while at basic pH, their deprotonation increases the density of negative charges, favoring cationic exchange with K^+ [18,19]. In our study, calcined clay (400 °C, 3 h) was impregnated with either K_2CO_3 or CH_3CO_2K, then tested in media at different pH. The results show that potassium dispersion is optimal under slightly basic conditions (pH 8) for both precursors, with a higher adsorption capacity for CH_3CO_2K, which can be explained by its greater solubility and better diffusion in the porous matrix [16]. At pH < 5, retention decreases significantly, which reflects the neutralization of exchange sites by protons. Between pH 6 and 9, a net increase in retention is observed, corresponding to the zone of maximum negative charge on the clay surface. For pH > 10, a slight decrease in capacity is recorded, possibly due to the precipitation of K_2CO_3 as KOH and the formation of insoluble carbonates or bicarbonates on the surface [13].

These results confirm that K^+ adsorption on calcined clay is governed by a balance between surface charge state and solution chemistry. The choice of precursor is also determining: potassium acetate, more soluble and less prone to alkaline precipitation, allows for a more homogeneous dispersion and a higher maximum capacity. This behavior is in agreement with the work of Ooi [15], who showed that adsorption of alkaline cations on modified clays presents an optimum in the pH range 8–9, and with that of Ahmaruzzaman [14], who emphasize the importance of the ionic state of the precursor in the kinetics and efficiency of impregnation.

Table 2
Effect of pH on K retention on clay impregnated with K_2CO_3 and CH_3CO_2K.

pH	q_e (mg g^{-1}) K_2CO_3	q_e (mg g^{-1}) CH_3CO_2K	Main Observation
3	45.2	58.4	Low adsorption, protonated sites
5	82.6	96.1	Increase, onset of OH deprotonation
7	125.3	146.5	Favorable adsorption, increased negative surface
8	149.8	198.9	Optimum observed, strong affinity of K^+ for exchange sites
9	146.1	192.4	Adsorption plateau
11	120.7	165.2	Slight decrease, possible formation of precipitates

3.4. Comparison of Agboville clay with other clays from Côte d'Ivoire, West Africa, and Africa

The mineralogical and physicochemical characteristics of clays vary significantly with their geological origin, influencing their capacity to retain metallic or alkaline species after thermal activation (Table 3). In Côte d'Ivoire, a comparison between the main deposits of Agboville (AGB), Bingerville (BIN), and Katiola (KAT) indicates that Agboville clay is predominantly kaolinitic (~75.5%), with low iron/goethite content, and contains ~14% illite and ~9% quartz. Its cation exchange capacity (CEC ~6.7 meq/100 g) is typical of kaolinite-rich materials and, combined with its good thermal stability, supports the formation of reactive metakaolinite and facilitates uniform K^+ retention after calcination [20].

Bingerville clay, also kaolinitic (CEC ~6.2 meq/100 g), contains higher amounts of iron oxides, which may interfere with alkaline ion dispersion during heating. Katiola clay, which contains a significant proportion of smectite (~20%) with a higher CEC (~35 meq/100 g), promotes efficient ion exchange but tends to undergo structural reorganizations upon calcination, which limit the stability of alkaline deposits [20, 21].

At the broader West African scale, Nigerian bentonites (montmorillonite-rich) exhibit high CEC and strong adsorption capacities for both organic and metallic species [23]. However, their swelling behavior and sensitivity to ionic strength often reduce the uniformity of alkaline ion distribution after impregnation [22]. In Burkina Faso, kaolins and lateritic clays show good potential after chemical activation, although their behavior upon alkaline deposition strongly depends on the intensity of pretreatment [24]. Activated kaolins from Ghana and Benin are mainly optimized for exchange and complexation processes rather than the stabilization of alkaline species.

Overall, while smectitic clays from West Africa perform well for ion exchange, Agboville kaolinitic clay offers a more favorable combination for stable and homogeneous potassium retention after calcination. This performance is linked to its dominant kaolinitic composition, low iron content, and good thermal stability. Experimentally, the optimal granulometry (100–250 µm) achieved the highest adsorption capacities 149.84 mg g^{-1} with K_2CO_3 and 198.91 mg g^{-1} with CH_3CO_2K surpassing values reported for several other Ivorian and regional deposits under comparable conditions.

In summary, the main criteria governing efficient potassium deposition after calcination are: (i) a thermally stable mineralogical composition that forms reactive metakaolinite without swelling, (ii) a low content of ferric and iron oxide phases that may hinder alkaline ion dispersion, (iii) a surface chemistry that becomes more reactive after thermal activation, and (iv) an optimized granulometry that ensures effective contact and controlled diffusion of precursor ions.

Agboville clay meets these conditions most effectively due to its predominantly kaolinitic composition, low iron content, and favorable thermal behavior. These characteristics explain its superior ability to retain potassium uniformly after calcination compared with other West African deposits [20, 24].

3.5. Influence of potassium precursor on K/Clay adsorption capacity

The nature of the potassium precursor strongly influences the solution chemistry (pH, ionic speciation), wetting behavior, and redistribution of ions during drying, thereby governing the dispersion and stabilization of K^+ on the calcined clay surface. Even at identical metal loadings, precursor effects, well documented in supported catalysis, remain decisive, particularly for acetate- and carbonate-based salts [25–27]. Potassium acetate (CH_3CO_2K) exhibits properties that promote efficient incorporation on calcined kaolinite in the 100–250 µm size range, mainly due to its high solubility, which ensures rapid and homogeneous contact with reactive surface groups.

Table 3
Synthetic comparison of Ivorian and West African clays for potassium deposition after calcination.

Origin and type of clay	Dominant mineralogy	CEC (meq/100 g)	Behavior upon K deposition after calcination
Agboville (CI)	Kaolinite ∼75%, illite ∼14%, quartz ∼9%, low Fe/goethite	∼6.7	Very favorable: clean, stable surface; homogeneous K dispersion (100–250 μm optimum)
Bingerville (CI)	Dominant kaolinite, higher goethite content	∼6.2	Moderate: Fe phases interfere with uniform dispersion
Katiola (CI)	Kaolinite + ∼20% smectite	∼35	High exchange capacity; lower stability upon calcination
Bentonite (Nigeria)	Montmorillonite-rich	>80	Excellent ion exchange; poor stability (swelling, salinity effects)
Kaolins (Burkina Faso)	Kaolinite/laterite	5–15	Performance dependent on chemical activation; moderate K retention stability

In addition, its clean thermal decomposition between 300 and 400 °C releases primarily H_2O, CO_2, and light volatile species, resulting in well-dispersed potassium species without persistent anionic residues. These characteristics facilitate the interaction of K^+ with surface hydroxyls and Lewis sites formed during dehydroxylation, improving the homogeneity of potassium retention after drying and calcination.

Conversely, potassium carbonate (K_2CO_3) presents specific limitations. Its high intrinsic alkalinity (pH ∼11.5) strongly influences surface charge, which can promote localized precipitation or uneven deposition during impregnation. In addition, the thermal stability of K_2CO_3 (persisting up to ∼890 °C) means that carbonate species can remain in the solid if surface reactions are not sufficient, potentially reducing the uniformity of potassium distribution. Achieving homogeneous dispersion with K_2CO_3 therefore requires stricter control of solution concentration, pH adjustment, drying rate, and thermal treatment [28, 29].

In summary, for calcined kaolinite in the 100–250 µm granularity range, CH_3CO_2K is the most efficient precursor, providing higher potassium loading and more uniform dispersion. This behavior is consistent with our experimental findings (higher adsorption capacities and more homogeneous EDS mapping) and with the literature on precursor effects in aluminosilicate-supported catalysts [25, 29].

3.6. Adsorption isotherm modeling for K^+/Clay (CH_3CO_2K, 100–250 µm)

The analysis of adsorption isotherms provides insight into the type of interactions established between K^+ ions and the clay surface after calcination and impregnation. The experimental equilibrium data obtained for the K_2CO_3- and CH_3CO_2K-doped clays (particle size 100–250 µm) were fitted us-

ing the Langmuir, Freundlich, and Temkin models (Table 4; Figures 2–4).

The Langmuir model, based on monolayer adsorption onto a surface with a finite number of uniform sites, yielded theoretical maximum capacities (q_m) of 149.84 mg g^{-1} for K_2CO_3 and 198.91 mg g^{-1} for CH_3CO_2K. However, the relatively low correlation coefficients (R^2 = 0.5246 and 0.5589) indicate that adsorption does not follow a strictly homogeneous monolayer mechanism and suggest the presence of heterogeneous binding sites [6].

The Freundlich model, which accounts for adsorption on heterogeneous surfaces and allows multilayer uptake, provided better fits, with R^2 values of 0.8308 (K_2CO_3) and 0.9249 (CH_3CO_2K). The n values greater than 1 (1.42 and 1.56) denote favorable adsorption, while the K_F constants (18.62 and 24.75) reflect the stronger affinity of CH_3CO_2K-treated clay for K^+ ions.

The Temkin model offered the best description of the experimental data, with R^2 = 0.9278 for K_2CO_3 and R^2 = 0.9894 for CH_3CO_2K. This model considers the progressive decrease in adsorption heat as the surface becomes occupied. The obtained constants B (212.02 and 184.70 J mol^{-1}) and K_T (0.0002 and 0.0003 L g^{-1}) confirm that adsorption proceeds through energetically non-uniform sites where adsorbate–adsorbent interactions vary with increasing surface coverage [7, 15].

Overall, the superiority of the Temkin model indicates that potassium adsorption on calcined Agboville clay involves heterogeneous energetic interactions rather than a purely monolayer process. The better fit obtained with CH_3CO_2K is consistent with its higher experimental adsorption capacity and more homogeneous potassium distribution.

All these results show that the granulometry $100 < X < 250$ µm offers an optimal compromise between specific surface area and internal porosity, allowing efficient diffusion of precursors into the porous matrix. The superiority of CH_3CO_2K in terms of adsorption capacity can be attributed to its greater solubility and better dispersion within the clay's porous structure [16].

These results corroborate the work of Alkhabbas [13], who highlighted that particle size and porosity strongly influence the adsorption capacity of modified clays, as well as that of Shaban [16], who demonstrated that thermal and chemical modification of kaolins and bentonites enhances the diversity and reactivity of surface sites.

The Temkin model thus appears to be the most relevant for describing potassium adsorption onto calcined clay, highlighting a process controlled by variable surface interactions, typical of heterogeneous materials.

3.7. Kinetic modeling of K^+/Clay adsorption (CH_3CO_2K, 100–250 µm)

The kinetic study describes the rate and mechanism of K^+ ion binding onto the surface of calcined clay impregnated with CH_3CO_2K. Three approaches were considered: the pseudo-first-order model [30], the pseudo-second-order model [9], and direct experimental observation (Table 5 and Figure 5). The pseudo-first-order model assumes that the adsorption rate is proportional to the number of available free sites, generally corresponding to physical adsorption on a homogeneous surface [7]. The pseudo-second-order model is based on the assumption that the rate-limiting step is chemisorption involving the sharing or exchange of electrons between K^+ ions and active surface groups. Experimental results show that the pseudo-second-order model best describes the process, with a correlation coefficient R^2 = 0.998 and excellent agreement between the theoretical adsorbed amount (q_e calc. = 198.9 mg g^{-1}) and the experimental value (q_e exp. = 198.9 mg g^{-1}). This agreement confirms that K^+ fixation is dominated by a chemical mechanism involving strong bonds with the hydroxyl and aluminosilicate groups of the clay [15, 16].

To complement the analysis, the temporal evolution of the adsorbed amount was compared to the values predicted by the models.

It can be observed that the pseudo-second-order model almost perfectly fits the experimental kinetics, including at short times (5–30 min) where adsorption is fastest, and during the equilibrium phase (60–720 min) where q_t remains constant. The pseudo-first-order model, although relatively close, tends to underestimate the initial adsorption rate and predict a plateau slightly lower than the experimental value. These results suggest that chemisorption is the dominant mechanism, with a secondary contribution from intra-particle diffusion in the initial phase. The granulometry $100 < X < 250$ µm optimizes the balance between specific surface area and pore accessibility, reducing mass transfer resistance and allowing homogeneous coverage of active sites by K^+ ions.

Table 4
Isotherm model parameters for K_2CO_3 and CH_3CO_2K on clay ($100 < X < 250$ μm).

Model	Parameter	K_2CO_3/Clay / CH_3CO_2K/Clay
Langmuir	q_m (mg g^{-1})	149.84 / 198.91
	K_L (L mg^{-1})	0.0035 / 0.0048
	R^2	0.5246 / 0.5589
Freundlich	K_F (mg g^{-1})(L mg^{-1})$^{1/n}$	18.62 / 24.75
	n	1.42 / 1.56
	R^2	0.8308 / 0.9249
Temkin	B (J mol^{-1})	212.02 / 184.70
	K_T (L g^{-1})	0.0002 / 0.0003
	R^2	0.9278 / 0.9894

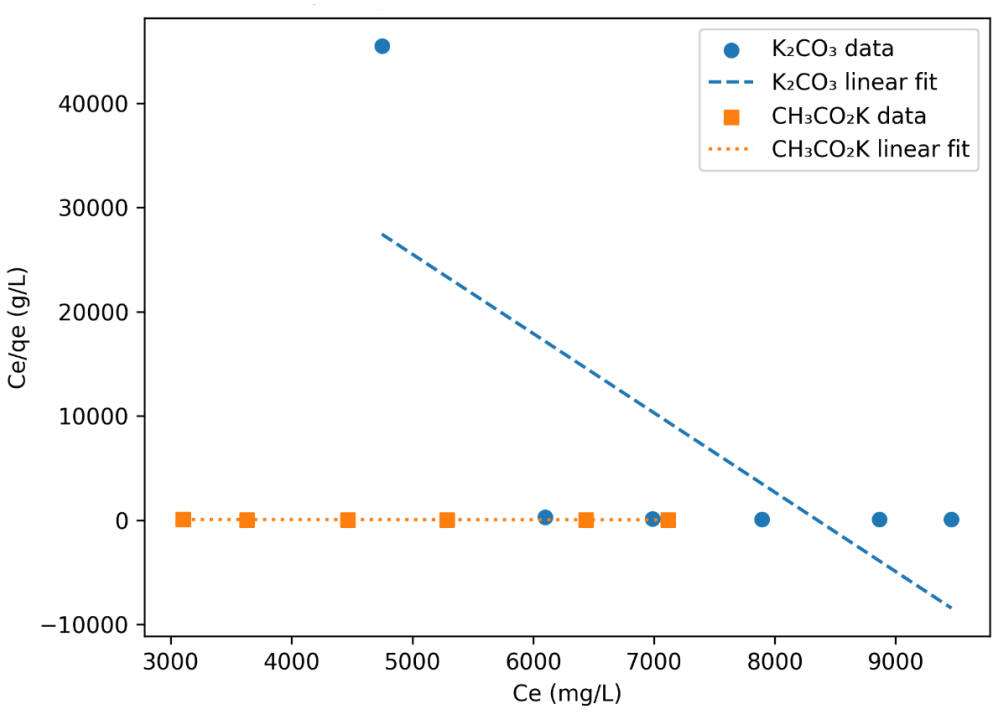

Fig. 2. Langmuir isotherms of K^+/Clay adsorption (100–250 µm).

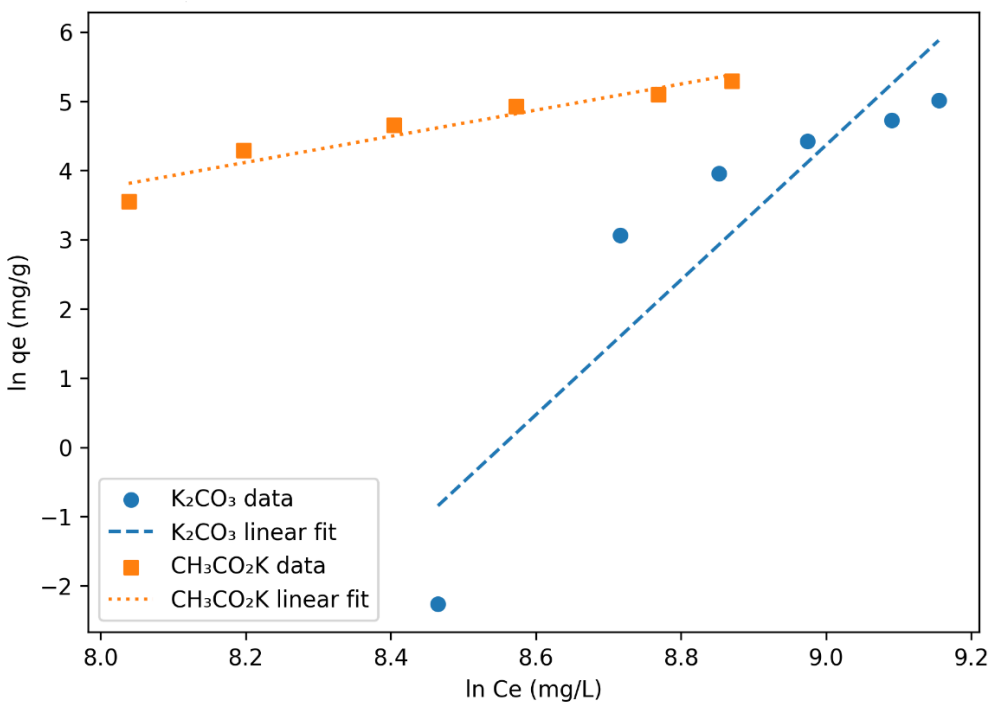

Fig. 3. Freundlich isotherms of K^+/Clay adsorption (100–250 µm).

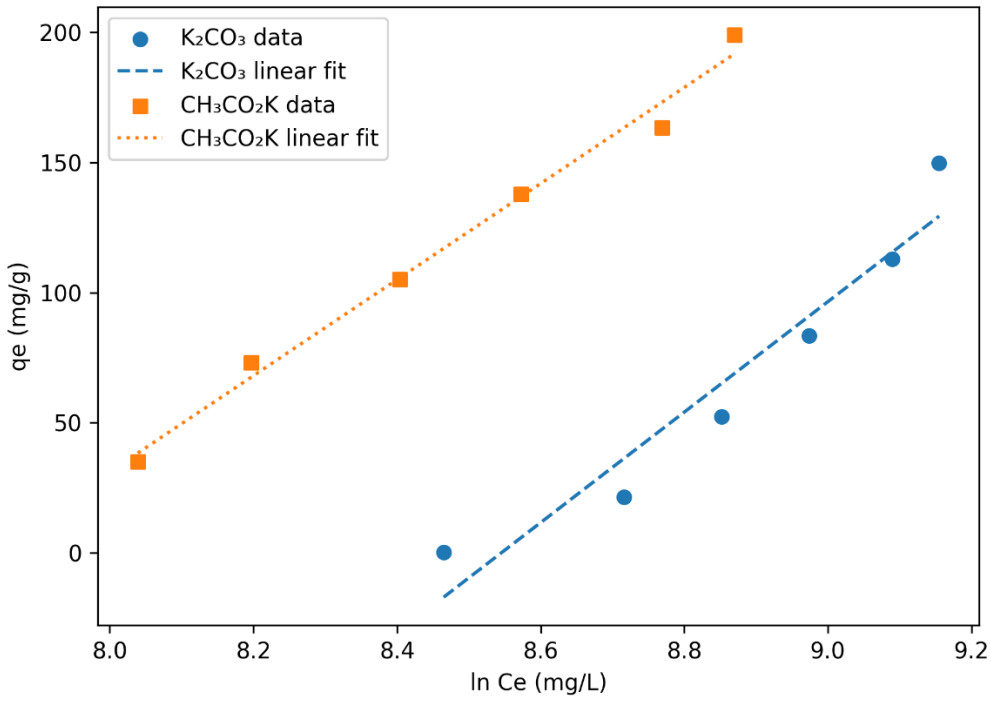

Fig. 4. Temkin isotherms of K^+/Clay adsorption (100–250 µm).

Recent studies confirm that thermal activation of clay followed by alkaline impregnation increases the proportion of high-energy sites, making chemisorption predominant [13, 15]. This configuration is particularly favorable for catalytic applications, where the stability and homogeneous distribution of potassium on the support are essential.

Table 5
Kinetic adsorption constants of K^+ on K/Clay (CH_3CO_2K, 100–250 μm).

Model	Parameters	Values	R^2
Pseudo-first order	k_1 (min^{-1})	0.031	0.942
	q_e calc. (mg g^{-1})	196.5	
Pseudo-second order	k_2 (g mg^{-1} min^{-1})	2.45×10^{-4}	0.998
	q_e calc. (mg g^{-1})	198.9	
Experimental	q_e exp. (mg g^{-1})	198.9	—

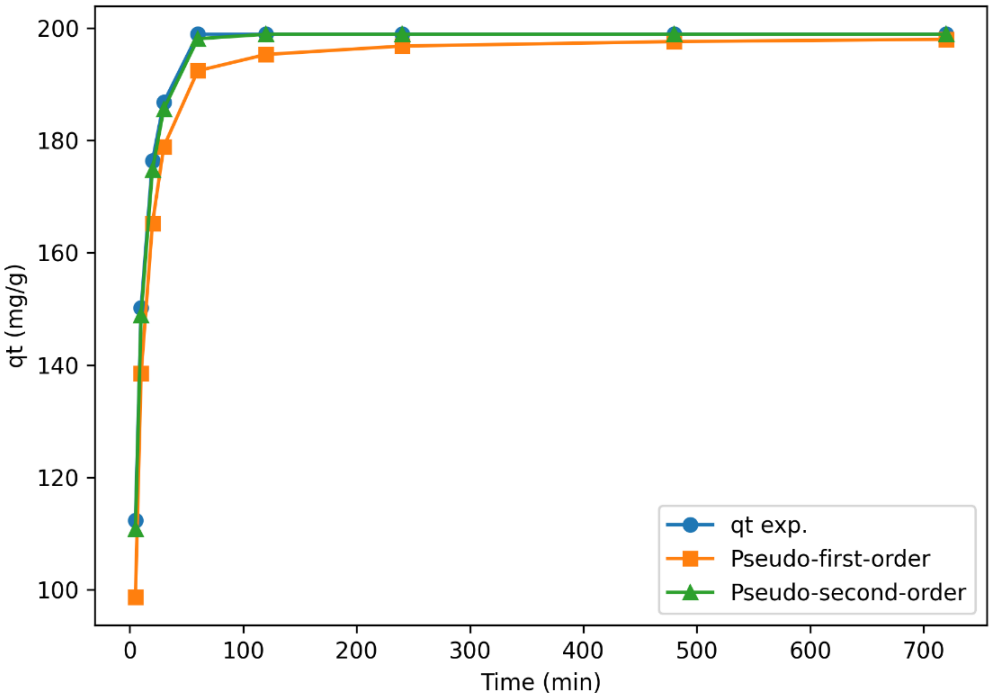

Fig. 5. Evolution of the adsorbed amount of K over time and comparison with kinetic models.

3.8. Thermodynamic model of K^+/Clay Adsorption (CH_3CO_2K, 100–250 µm)

Thermodynamic analysis complements the isothermal and kinetic study by assessing the feasibility (ΔG°), energetic nature (ΔH°), and interfacial order (ΔS°) of the K^+/calcined clay impregnated with CH_3CO_2K system. On activated aluminosilicates, the expected trend is confirmed: $\Delta G^\circ < 0$ (spontaneity), $\Delta H^\circ > 0$ moderate (endothermicity linked to partial desolvation of K^+ and strengthening of surface-K^+ interactions), and $\Delta S^\circ > 0$ (release of structured water and increase in interfacial disorder), in agreement with recent literature [16]. The table below summarizes the main experimental data (Table 6 and Figure 6).

In line with activated cation–clay systems, the expected thermodynamic trends are observed: $\Delta G^\circ < 0$ confirming spontaneity, $\Delta H^\circ > 0$ of moderate magnitude indicating an endothermic process linked to the partial dehydration of K^+ and the strengthening of surface-K^+ interactions, and $\Delta S^\circ > 0$ reflecting the release of structured water and the increase in interfacial disorder.

Table 6
Thermodynamic adsorption parameters for K^+/Clay.

Temperature (K)	K_c	$\ln K_c$	ΔG° (kJ mol^{-1})
298	12.0	2.485	-6.16
308	15.0	2.708	-6.93
318	19.0	2.944	-7.78
328	23.0	3.135	-8.55

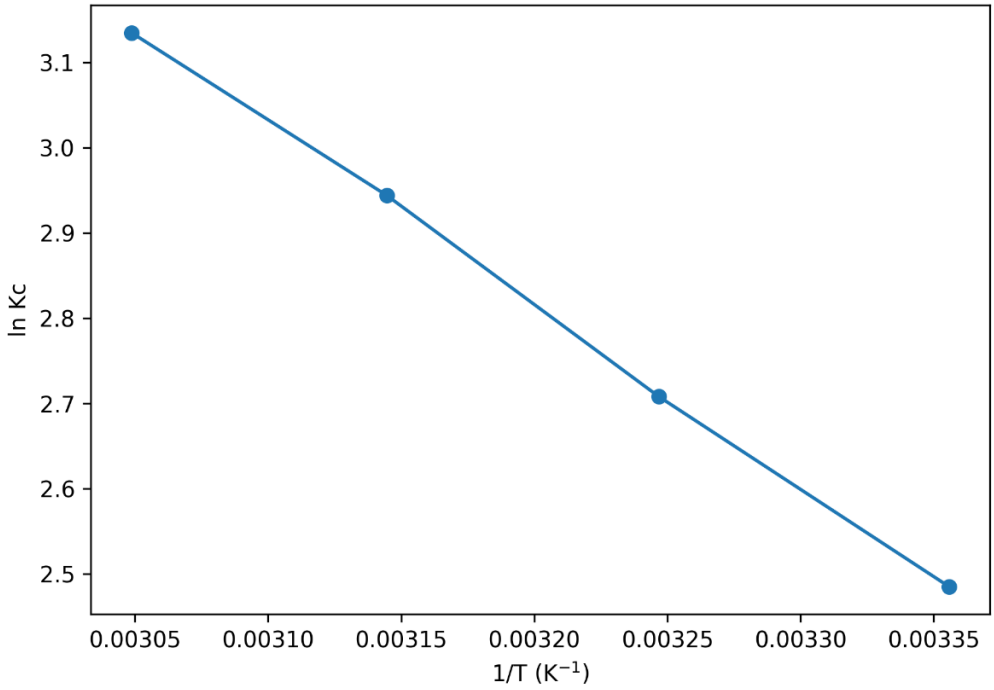

Fig. 6. Van't Hoff Plot for K^+/Clay.

For the optimal granulometry 100–250 µm, the Van't Hoff regression over 298–328 K yields $\Delta H^\circ \approx +17.8$ kJ mol^{-1} and $\Delta S^\circ \approx +80.3$ J mol^{-1} K^{-1}, while the equilibrium constant K_c increases with temperature. From a physicochemical standpoint, the negative ΔG° values across the entire range confirm the feasibility of K^+ deposition; the moderate endothermicity and the increase of K_c with T are consistent with K^+ desolvation and the activation of high-energy sites generated by calcination; the positive ΔS° reflects a favorable interfacial reorganization through the desorption of bound water and improved local mobility [13, 15].

This triptych ($\Delta G^\circ < 0$; $\Delta H^\circ > 0$; $\Delta S^\circ > 0$), typical of activated cation–clay systems, supports the ability of the CH_3CO_2K/clay (100–250 µm) system to ensure both stable and energetically favorable potassium dispersion, in agreement with recent findings on modified aluminosilicate supports and potassium-doped clays for catalytic applications, as well as with the isotherm and kinetic analyses (pseudo-second-order fit and higher capacity with CH_3CO_2K) and the reference literature on adsorption and modeling [10, 11].

3.9. Characterization of the obtained material K/Clay-CH_3CO_2K

3.9.1. Point of Zero Charge (pH_{PZC})

The point of zero charge (pH_{PZC}) characterizes the acid–base nature of clay surfaces and their ability to interact with ions [7]. It corresponds to the pH at which the net surface charge is zero, i.e., when acidic (≡Si–OH, ≡Al–OH) and basic (≡Si–O^-, ≡Al–O^-) sites are balanced (Figure 7). The raw Agboville clay shows a pH_{PZC} of 4.6, typical of moderately acidic natural kaolinites [18]. After calcination at 400 °C, this value slightly increases to 5.1, due to partial dehydroxylation and the formation of exposed Al^{3+} Lewis sites in the metakaolinite phase [31, 32]. A more pronounced rise to 6.2 is observed after potassium doping (CH_3CO_2K), indicating the neutralization of acidic sites and the creation of basic centers (≡O^-K^+) capable of interacting with cations or polar molecules [16].

These results, consistent with Tran [33], demonstrate that K^+ doping increases the surface basicity and reactivity, thereby improving the material's adsorption performance in neutral to slightly basic environments.

3.9.2. Fourier Transform Infrared Spectroscopy (FT-IR)

FT-IR analysis highlights the evolution of kaolinite functional groups during calcination and potassium doping. The spectra recorded between 4000 and 400 cm^{-1} (Figure 8) reveal structural changes related to transformation and potassium fixation. The ν(OH) bands at 3695 and 3620 cm^{-1}, characteristic of internal and surface hydroxyl groups, decrease sharply after calcination at 400 °C, indicating partial dehydroxylation and the formation of an amorphous metakaolinite phase [18, 31]. This transformation favors the appearance of Lewis acid sites and more reactive Si–O–Al linkages, promoting K^+ incorporation [13]. The main ν(Si–O) band near 1030 cm^{-1} broadens and shifts slightly to 1010–1005 cm^{-1}, suggesting disruption of the SiO_4 network and possible formation of K–O–Si bonds [19, 32]. This shift, also observed in alkali-metal-doped clays [31, 32], indicates a strong interaction between potassium and the aluminosilicate framework.

Furthermore, the acetate (1550–1410 cm^{-1}) and carbonate (1460–870 cm^{-1}) group bands disappear after recalcination at 350–400 °C, confirming the elimination of organic ligands and the stabilization of K^+ species within the matrix [26, 27].

Overall, these changes demonstrate that potassium is firmly incorporated into the aluminosilicate structure rather than merely adsorbed on the surface, producing a stable and functionalized material whose modified surface exhibits favorable acid–base properties for adsorption applications.

3.9.3. Elemental Analysis by EDS Spectroscopy

Elemental Analysis by EDS Spectroscopy was used to determine the chemical composition and spatial distribution of potassium in the doped materials. The spectra and elemental maps (Figure 9) confirm the presence of the dopant and the stability of the aluminosilicate framework. The raw and calcined clay samples contain only 0.1–0.2 at.% of K, corresponding to natural traces of feldspar or illite [18]. After doping with CH_3CO_2K, the potassium content rises to 1.0–3.0 at.%, confirming the effective incorporation of K^+ onto the thermally activated clay surface, in agreement with observations reported in previous studies [13, 34].

The elemental mapping shows a homogeneous distribution of K signal (CV $< 15\%$), particularly clear for the acetate-derived material, where the uniform dispersion reflects a more efficient ion-exchange kinetics [26, 27]. No agglomerate formation was detected, confirming a stable and uniform surface distribution of potassium. The atomic ratios K/Si and K/Al (~0.02–0.05) indicate that potassium is predominantly associated with surface sites of the thermally activated clay, in agreement with observations reported in previous studies [31, 32].

These results confirm the good disper-

sion of K^+, in full agreement with FT-IR and thermogravimetric analyses, and demonstrate the successful potassium doping without any structural degradation of kaolinite.

3.9.4. Thermogravimetric Analysis (TGA)

The Thermogravimetric analysis (TGA) was performed to evaluate the thermal stability and decomposition behavior of the clay before and after potassium doping. The obtained curves (Figure 10) reveal four main stages: (1) Between 25 and 150 °C, a 3–5% weight loss associated with the removal of physically adsorbed water; (2) Between 200 and 400 °C, the decomposition of organic residues from acetate ligands of the CH_3CO_2K precursor; (3) Between 400 and 650 °C, the dehydroxylation of kaolinite into metakaolin, with a weight loss of 8–10% associated with a temperature between 520–550 °C; and (4) Above 700 °C, the thermal stabilization of the amorphous matrix. After doping and post-treatment, the losses associated with precursor residues disappear, confirming the stable incorporation of K^+ and the absence of carbonate or organic remnants. This behavior indicates an enhanced thermal resistance and neutralization of acidic sites by potassium, in agreement with Djomgoue [34], who reported that alkali dopants improve the structural stability and basicity of activated clays.

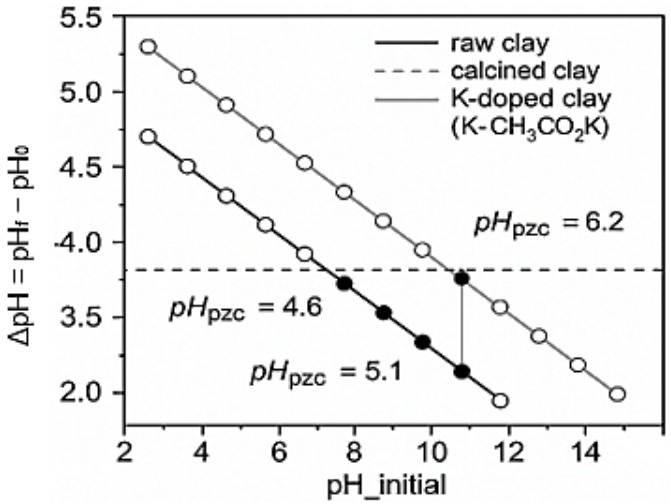

Fig. 7. pH_{PZC} determination curves ($\Delta pH = f(pH_0)$) for raw, calcined and K/Clay.

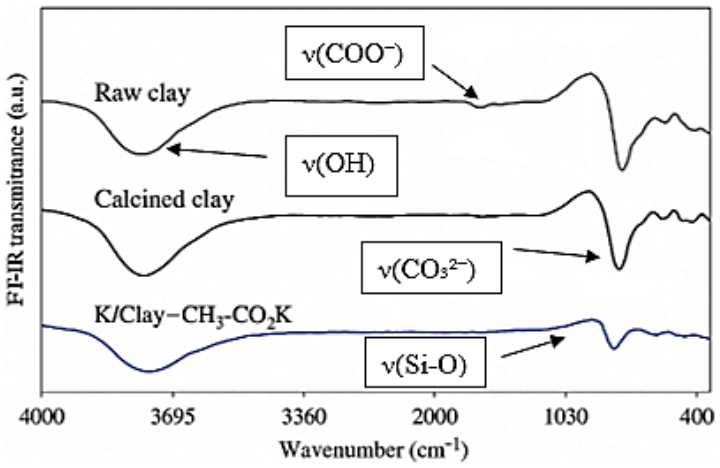

Fig. 8. FT-IR spectra recorded at the different stages of clay modification.

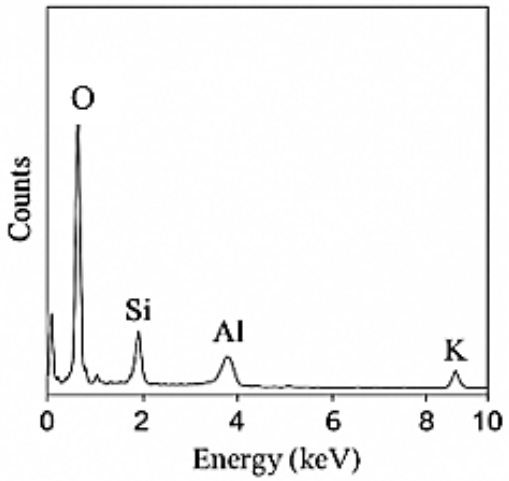

Element	Atomic %
Si	19.3
Al	18.6
O	61.2
K	0.9

Fig. 9. EDS spectrum of the K/Clay-CH_3CO_2K doped material and atomic composition.

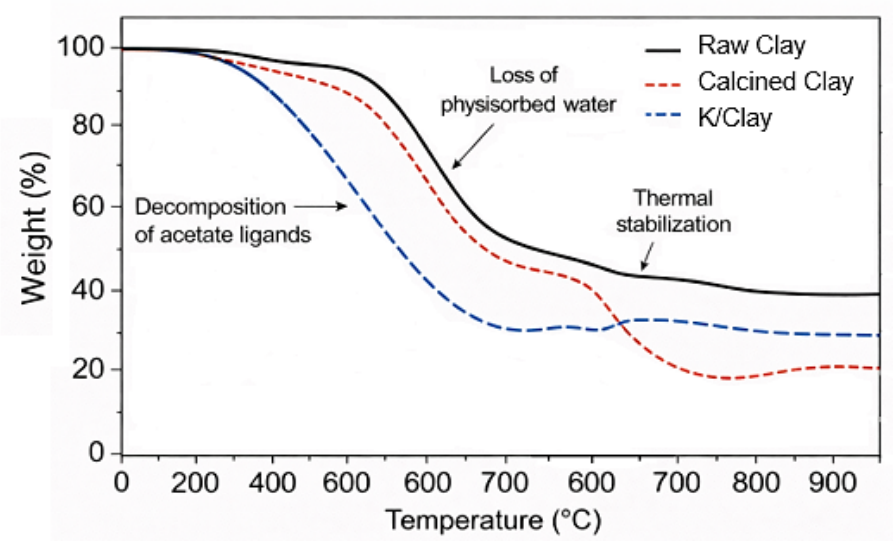

Fig. 10. Comparative TGA curves of the raw clay, calcined clay and K/Clay.

4. Conclusion

This study demonstrated the effectiveness of potassium doping of thermally activated kaolinitic clay from Agboville for the retention of K^+ ions in aqueous media. Particle size was identified as a key parameter, with the 100–250 µm fraction providing the best performance. Maximum adsorption capacities reached 149.84 mg g^{-1} for K_2CO_3 and 198.91 mg g^{-1} for CH_3CO_2K, the latter yielding the highest affinity for K^+ and the most uniform distribution of potassium on the clay surface.

Isotherm modeling showed that the Temkin model best described the equilibrium behavior ($R^2 = 0.9894$ for CH_3CO_2K), suggesting heterogeneous interaction energies across the surface. Kinetic analysis revealed that adsorption followed the pseudo-second-order model ($R^2 = 0.998$), with excellent agreement between experimental and calculated equilibrium values ($q_e = 198.9$ mg g^{-1}), confirming that chemisorption is the dominant process. Thermodynamic parameters ($\Delta G°$ from -6.16 to -8.55 kJ mol^{-1}, $\Delta H° = +17.8$ kJ mol^{-1}, $\Delta S° = +80.3$ J mol^{-1} K^{-1}) indicated that adsorption is spontaneous, endothermic, and accompanied by increased disorder at the solid–liquid interface.

Characterization analyses supported these findings. FT-IR revealed attenuation of structural ν(OH) bands (3695–3620 cm^{-1}) and a shift of the ν(Si–O) vibration toward ~1010 cm^{-1}, consistent with interactions be-

tween potassium ions and aluminosilicate groups. The pH_{PZC} increase from 4.6 to 6.2 confirmed the enhanced basicity of the doped clay. EDS measurements showed homogeneous potassium incorporation at levels ranging from 1.0 to 3.0 at.% (CV < 15%), while TGA confirmed the removal of precursor residues and the thermal stability of the modified material above 700 °C.

Overall, potassium doping, particularly using CH_3CO_2K, produces a thermally robust, chemically stable, and highly basic clay material. These characteristics make potassium-modified Agboville clay a cost-effective candidate for use as an adsorbent and catalytic support in water treatment and environmental remediation applications.

References

[1] S. Hamdi, A. Míguez-González, R. Cela-Dablanca, A. Barreiro, *Natural and modified clays as low-cost and ecofriendly materials to remove salinomycin from environmental compartments*, Journal of Environmental Management 368 (2024) 122158. https://doi.org/10.1016/j.jenvman.2024.122158

[2] A. Ochirkhuyag, J. Temuujin, *The catalytic potential of modified clays: A review*, Minerals 14 (2024) 629. https://doi.org/10.3390/min14060629

[3] A. Alvarez-Coscojuela, J. Marco-Gibert, J. Mañosa, J. Formosa, J.M. Chimenos, *Thermal activation of kaolinite through potassium acetate intercalation: A structural and reactivity study*, Applied Clay Science 259 (2024) 107515. https://doi.org/10.1016/j.clay.2024.107515

[4] I. Aitor Polcowñuk Iriarte, A. Mocciaro, N. Maximiliano Rendtorff, D. Richard, *Dehydroxylation of kaolinite: evaluation of activation energy by thermogravimetric analysis and density functional theory insights*, Minerals 15 (2025) 607. https://doi.org/10.3390/min15060607

[5] K. Scrivener, K. Martirena, S. Bishnoi, S. Maity, *Calcined clay limestone cements (LC³)*, Cement and Concrete Research 114 (2018) 49–56. https://doi.org/10.1016/j.cemconres.2017.08.017

[6] K.Y. Foo, B.H. Hameed, *Insights into the modeling of adsorption isotherm systems*, Chemical Engineering Journal 156 (2010) 2–10. https://doi.org/10.1016/j.cej.2009.09.013

[7] N. Ayawei, A.N. Ebelegi, D. Wankasi, *Modelling and interpretation of adsorption isotherms*, Journal of Chemistry 2017 (2017) 3039817. https://doi.org/10.1155/2017/3039817

[8] M.A. Hubbe, S. Azizian, S. Douven, *Implications of apparent pseudo-second-order adsorption kinetics onto cellulosic materials: A review*, BioResources 14 (2019) 7582–7626. https://doi.org/10.15376/biores.14.3.7582-7626

[9] Y.S. Ho, G. McKay, *Pseudo-second order model for sorption processes*, Process Biochemistry 34 (1999) 451–465. https://doi.org/10.1016/S0032-9592(98)00112-5

[10] E.C. Lima, A. Hosseini-Bandegharaei, M. Anastopoulos, *A critical review of the estimation of thermodynamic parameters in adsorption studies*, Journal of Molecular Liquids 273 (2019) 425–434. https://doi.org/10.1016/j.molliq.2018.10.048

[11] H.N. Tran, S.-J. You, A. Hosseini-Bandegharaei, H.-P. Chao, *Mistakes and inconsistencies regarding adsorption isotherms and kinetics*, Water Research 120 (2017) 88–116.

https://doi.org/10.1016/j.watres.2017.04.014

[12] H.N. Tran, N.P. Thanh Trung, E.C. Lima, J.-C. Bollinger, N. Duy Dat, H.-P. Chao, R.-S. Juang, *Revisiting the calculation of thermodynamic parameters of adsorption processes from the modified equilibrium constant of the Redlich-Peterson model*, Journal of Chemical Technology & Biotechnology 98 (2023) 462–472. https://doi.org/10.1002/jctb.7258

[13] M. Alkhabbas, A.M. Al-Ma'abreh, G. Edris, T. Saleh, H. Alhmood, *Adsorption of Anionic and Cationic Dyes on Activated Carbon Prepared from Oak Cupules: Kinetics and Thermodynamics Studies*, International Journal of Environmental Research and Public Health 20 (2023) 3280. https://doi.org/10.3390/ijerph20043280

[14] M. Ahmaruzzaman, *Adsorption of heavy metals from aqueous solution by low-cost adsorbents: A review*, Advances in Colloid and Interface Science 166 (2011) 36–59. https://doi.org/10.1016/j.cis.2011.04.005

[15] H.K. Ooi, X.N. Koh, H.C. Ong, H.V. Lee, M.S. Mastuli, Y.H. Taufiq-Yap, F.A. Alharthi, A.A. Alghamdi, N.A. Mijan, *Progress on modified calcium oxide derived waste-shell heterogeneous catalysts for biodiesel production*, Catalysts 11 (2021) 194. https://doi.org/10.3390/catal11020194

[16] M. Shaban, R. El-Raey, M. Rabia, *Potassium-modified clays as efficient heterogeneous catalysts for biodiesel production*, Renewable Energy 181 (2022) 922–933. https://doi.org/10.1016/j.renene.2021.09.042

[17] M.A.H. Lokman NolHakim, N.A. Mohd Shohaimi, W.N. Aini Wan Mokhtar, M. Lokman Ibrahim, R.F. Abdullah, *Immobilization of potassium-based heterogeneous catalyst over alumina beads and powder support in the transesterification of waste cooking oil*, Catalysts 11 (2021) 976. https://doi.org/10.3390/catal11080976

[18] J. Hua, M. Ji, P. Jiao, Z. Yin, Q. Xia, L. Jiang, J. Zhang, H. Pan, *Heterogeneous acid catalysts for biodiesel production: Effect of physicochemical properties on their activity and reusability*, Catalysts 15 (2025) 396. https://doi.org/10.3390/catal15040396

[19] R.F. Botti, M.D.M. Innocentini, T.A. Faleiros, M.F. Mello, D.L. Flumignan, L.K. Santos, G. Franchin, P. Colombo, *Biodiesel processing using sodium and potassium geopolymer powders as heterogeneous catalysts*, Molecules 25 (2020) 2839. https://doi.org/10.3390/molecules25122839

[20] H. Wang, Y. Wang, D.D. Dionysiou, *Advanced oxidation processes for removal of emerging contaminants in water*, Water 15 (2023) 398. https://doi.org/10.3390/w15030398

[21] A. Sanogo, A. Ouédraogo, I. Kaboré, *Activation and characterization of Burkina Faso kaolins for adsorption applications*, Journal of Environmental Chemical Engineering 11 (2023) 109876. https://doi.org/10.1016/j.jece.2023.109876

[22] M. Liu, S. Zhang, Z. Wang, *Advanced oxidation processes of organic contaminants*, Toxics 12 (2024) 579. https://doi.org/10.3390/toxics12080579

[23] K.C. Igwilo, N. Uwaezuoke, N. Okoli, F.T. Obasi, E.E. Okoro, *Beneficiation of Nigerian bentonite using local materials: Characterization and rheological*

evaluation, Journal of Petroleum Exploration and Production Technology 10 (2020) 3399–3407. https://doi.org/10.1007/s13202-020-00956-8

[24] M. Djebbar, F. Djafri, *Adsorption of zinc ions in water on natural and treated clay*, Chemistry and Chemical Technology 12 (2018) 272–278. https://doi.org/10.23939/chcht12.02.272

[25] P. Munnik, P.E. de Jongh, K.P. de Jong, *Recent developments in the synthesis of supported catalysts*, Chemical Reviews 115 (2015) 6687–6718. https://doi.org/10.1021/cr500486u

[26] X. Wei, L. Zhang, Y. Zhao, *Effect of precursor type on metal dispersion over oxide supports: A comparative study*, Catalysis Today 388 (2021) 72–81. https://doi.org/10.1016/j.cattod.2021.05.011

[27] F. Winter, M.M. Rahman, L. Giebeler, *Acetate precursors for uniform metal dispersion on oxide and aluminosilicate supports*, Microporous and Mesoporous Materials 379 (2024) 112489. https://doi.org/10.1016/j.micromeso.2023.112489

[28] H. Cheng, Q. Liu, J. Yang, Q. Zhang, R.L. Frost, *Mechanism of dehydroxylation temperature decrease and high-temperature phase transition of kaolinite intercalated by potassium acetate*, Journal of Colloid and Interface Science 378 (2012) 104–110. https://doi.org/10.1016/j.jcis.2012.02.065

[29] L. Espinosa-Alonso, *Drying of impregnated γ-Al_2O_3: Effects on distribution and interaction of Ni salts*, Journal of Physical Chemistry C 112 (2008) 7201–7209. https://doi.org/10.1021/jp710676v

[30] S. Azizian, *Kinetic models of sorption: A theoretical analysis*, Chemical Engineering Journal 104 (2004) 27–35. https://doi.org/10.1016/j.cej.2004.07.006

[31] D. Precious Kgabi, A. Ataro Ambushe, *Removal of Pb(II) ions from aqueous solutions using natural and HDTMA-modified bentonite and kaolin clays*, Heliyon 10 (2024) e38136. https://doi.org/10.1016/j.heliyon.2024.e38136

[32] B.E. Azanfire, D. Bulgariu, N. Cimpoeşu, L. Bulgariu, *Efficient Removal of Toxic Heavy Metals on Kaolinite-Based Clay: Adsorption Characteristics, Mechanism and Applicability Perspectives*, Water 17 (2025) 1938. https://doi.org/10.3390/w17131938

[33] H.N. Tran, *On the calculation of thermodynamic parameters in adsorption studies: The importance of properly defining the equilibrium constant*, Journal of Molecular Liquids 344 (2021) 117700. https://doi.org/10.1016/j.molliq.2021.117700

[34] P. Djomgoue, D. Njopwouo, *FT-IR spectroscopy applied for surface clays characterization*, Journal of Surface Engineered Materials and Advanced Technology 3 (2013) 275–282. http://dx.doi.org/10.4236/jsemat.2013.34037